Microchim Acta (2017) 184:4785–4792
DOI 10.1007/s00604-017-2523-6

ORIGINAL PAPER

Colorimetric immunoassay for rapid detection of *Vibrio parahaemolyticus*

Yushen Liu[1] · Chao Zhao[1] · Xiuling Song[1] · Kun Xu[1] · Juan Wang[1] · Juan Li[1]

Received: 27 June 2017 / Accepted: 18 September 2017 / Published online: 3 October 2017

Abstract *Vibrio parahaemolyticus* (*V. parahaemolyticus*) is one of the most common food-borne pathogens. The authors describe a rapid colorimetric assay for *V. parahaemolyticus* that is based on a combination of a magnetic bead-based sandwich immunoassay and signal amplification via an enzmye mimic. MnO_2 nanoparticles are used as an artificial oxidase that oxidizes 3,3′,5,5′-tetramethylbenzidine in the presence of oxygen to form a blue (and readily visible) product with an absorption maximum at 652 nm. By combining the superior capture efficiency of magnetic beads with the high catalytic activity of the enzmye mimic, this method can detect *V. parahaemolyticus* concentration in the range between 10 to 10^5 cfu·mL^{-1} without pre-enrichment, and the limit of detection is as low as 10 cfu·mL^{-1}. Recoveries ranging from 87.5% to 106.0% are found when analyzing spiked oyster samples. The assay is rapid, sensitive, and specific and specific. In our perception, it shows promise in rapid instrumental and on-site visual detection of *V. parahaemolyticus*.

Keywords Food safety · *Vibrio parahaemolyticus* · Oyster · Visual detection · Immunomagnetic separation · Artificial enzyme

Yushen Liu and Chao Zhao contributed equally to this work.

Electronic supplementary material The online version of this article (https://doi.org/10.1007/s00604-017-2523-6) contains supplementary material, which is available to authorized users.

✉ Juan Wang
jwang0723@jlu.edu.cn

✉ Juan Li
li_juan@jlu.edu.cn

[1] School of Public Health, Jilin University, Changchun, Jilin, China

Introduction

Vibrio parahaemolyticus (*V. parahaemolyticus*) is a Gram-negative and facultative halophilic bacterium, and frequently found in zooplankton, coastal fish, and shellfish (especially oysters) [1]. A series of clinical symptoms can be caused by consuming raw or undercooked seafood contaminated with *V. parahaemolyticus*, including watery diarrhea, abdominal cramps, nausea, vomiting, headache, low fever, and even bloody diarrhea [2, 3]. Due to the widespread distribution in the coastal and marine waters, *V. parahaemolyticus* is not only the leading cause of seafood-associated bacterial gastroenteritis in the United States [4], but it is also one of the most important food-borne pathogens in Asia, resulting in approximately half of the food poisoning outbreaks in China, Japan, and several Southeast Asian countries [2, 5]. Studies indicate that *V. parahaemolyticus* can grow up to 1000-fold in 2–3 h at room temperature [6]. Therefore, it is critical to develop methods and strategies for sensitive and rapid detection of *V. parahaemolyticus*.

Traditionally, a series of culture-based biochemical methods has been widely used for isolation and identification of *V. parahaemolyticus* strains. As the gold-standard, these methods generally require time-consuming and laborious steps [7]. In order to shorten the analysis time and improve the detection efficiency, several strategies based on the polymerase chain reaction (PCR) have been developed for targeting specific genes of *V.parahaemolyticus* [8]. However, PCR methods are still restricted by the need for professional operators and special equipment [9]. To overcome these limitations, various rapid testing methods based on the immunomagnetic separation (IMS) technologies have been established, which using magnetic beads coated with specific antibodies (IMBs) to capture and remove pathogens from the complex matrices by an external magnetic field [10, 11].

Colorimetric analytical strategies based on immunomagnetic ELISA system have aroused special attention due to no requirement for any advanced apparatus, and become an attractive and cost-effective detection assay [12, 13]. All these advantages make colorimetric assay for effective detection of bacterial contamination in food samples.

To date, various types of MnO_2 nanomaterials were reported to possess intrinsic oxidase-like activity [14], which can catalytically oxidize the substrate 3,3′,5,5′-tetramethylbenzidine (TMB), generating a high visibility optical signal. Since the catalytic activity of MnO_2 nanomaterials as a mimic enzyme depends on dissolved molecular oxygen in the solution [15], rather than H_2O_2 served as enzyme substrate, and the MnO_2-TMB platform has been proposed as a potential detection system for instead of conventional horseradish peroxidase (HRP)-TMB-H_2O_2 system. Indeed, the system has been applied to quantitatively measure any inhibitor of TMB oxidation including H_2O_2 and glucose in blood [16], glutathione [14], and ascorbic acid [17]. Therefore, the previous findings showed that MnO_2 nanomaterials are highly recommended as a novel and facile tool for colorimetric detection.

In the present study, we aimed to develop a fast and reliable method for colorimetric determination of *V. parahaemolyticus*. The integrated method proposed to combine the advantages of the highly efficient immunomagnetic separation and the remarkable catalytic activity of MnO_2 nanoparticles for the oxidation of TMB. Sandwich complexes of immunomagnetic beads, *V. parahaemolyticus*, and MnO_2 nanoparticles would be formed based on and the recognition of antibodies and target. In the addition of TMB, the colour variations ranging from light to deep blue were directly proportional to the concentration of bacteria. Additionally, the visualization results endow the colorimetric assay potency for high sensitive and selective detection of *V. parahaemolyticus* in oyster samples.

Materials and methods

Materials and reagents

Rabbit IgG antibodies and chicken egg yolk antibodies (IgY) were prepared in our own laboratory according to our previous work [18, 19], and the purities of the IgG and IgY were analyzed by sodium dodecyl sulfate polyacrylamide gel electrophoresis (SDS-PAGE) (Fig. S1). Synthesis of citric acid coated Fe_3O_4 nanoparticles (MNP-CA) [20] and BSA-templated MnO_2 nanoparticles (BSA-MnO_2 NPs) [15] were explained in detail in electronic supplementary material (ESM). Double-distilled water and phosphate-buffered saline (PBS, 0.01 mol· L^{-1}, pH 7.4) were prepared by us. All other the chemicals and reagents employed were of analytical grade and were used without any further purification.

Bacteria culture

All the bacterial strains used in this study were provided by the Department of Hygienic Inspection, School of Public Health, Jilin University (Changchun, China). *Vibrio parahaemolyticus*-strain (*V. parahemolyticus*, ATCC17802) was grown in Tryptone Soya Broth supplemented with 3.0% NaCl and incubated at 37 °C with shaking at about 250 rpm for about 18 h. Other bacteria including *Salmonella typhimurium* (*S. typhimurium*, ATCC13311), *Shigella Bogdii* (*S. Bogdii*, ATCC9207) *Escherichia coli O157:H7* (*E. coli O157:H7*, ATCC25922), *Staphylococcus aureus* (*S. aureus*, ATCC49775) and *Listeria monocytogenes* (*L. monocytogenes*, ATCC19111) were cultured in Luria-Bertani medium under aerobic conditions at 37 °C for 18 h to 20 h. The concentrations of bacteria were determined on the standard plate count agar using plate counting method [21].

Instrumentations

The UV-vis absorption spectra were measured with a spectrophotometer (TU-1810 DPC Persee, Beijing, China) using a 1 cm path-length quartz cell. Transmission electron microscopy (TEM) images and high-resolution transmission electron microscopy (HRTEM) images of nanoparticles were performed on a JEOL JEM-2100F transmission electron microscope operated at an accelerating voltage of 200 kV (Tokyo, Japan). Fourier transform infrared (FTIR) spectra in the region from 4000 to 500 cm-1 were recorded as KBr discs on a Nicolet 6700 FTIR spectrometer (Thermo Inc., USA) for evaluating various encapsulated nanoparticles. The zeta potential measurements were determined using a zeta potential analyser (NanoBrook 90Plus Zeta, Brookhaven, USA). Magnetic hysteresis loops were measured with a vibrating sample magnetometer (Lake Shore 7410 VSM).

Synthesis of IgG-conjugated MNP-CA (MNP-CA-IgG)

In this work, MNP-CA was synthesized by solvothermal method [20], using CA as a coating ligand for enhancing stability and biocompatibility. For specific recognition and capture of target bacteria, MNP-CA-IgG were fabricated according to the method described in the literature [22]. Typically, 5 mg of the synthesized MNP-CA were dispersed in 1 mL of PBS (0.01 M, pH 7.4) containing 10 mg EDC and 5 mg NHS. The mixture was shaken gently at room temperature for activating the carboxyl groups on the magnetic nanosphere surface. After 0.5 h incubation, the nanospheres were harvested and washed with PBS three times by magnetic separation, which were then dispersed in 1.0 mL of PBS to react with 500 μg of rabbit IgG antibodies for about 2 h with continuous shaking at room temperature. Then, the resultant products were washed with PBS to remove surplus antibody, and

blocked with 1% BSA-PBS for 1 h at room temperature with gentle agitation. Finally, the MNP-CA-IgG were stored in PBS at 4 °C before use.

Synthesis of IgY-conjugated BSA-MnO_2 NPs (IgY-BSA-MnO_2 NPs)

A biotemplated synthesis of BSA-MnO_2 NPs were conjugated with IgY antibodies using the cross-linker EDC [15, 23]. For this process, 0.5 mL BSA-MnO_2 nanoparticles stock solution were mixed with 1.5 mL PBS, and then 1 mg EDC and 1.5 mg NHS were added at room temperature with continuous stirring for 15 min. Thereafter, 50 mg IgY antibodies were added and incubated for 2 h. The precipitated IgY-BSA-MnO_2 NPs was successfully obtained after centrifugation at 15000 rpm for 30 min to remove excess IgY antibodies and reagents.

Detection of *V. parahaemolyticus*

Bacteria samples with varying concentrations (0, 10, 25, 50, 75, 100, 500, 1000, 5000, 10,000, 50,000 and 100,000 cfu·mL^{-1}) were prepared by diluting the freshly cultured bacteria with sterile PBS. After optimization of experimental conditions, each *V. parahaemolyticus* standard solution (100 μL) was added into the mixture solution, which a total of 900 μL aqueous solution containing 0.5 mg MNP-CA-IgG and 1 mg IgY-BSA-MnO_2 NPs. And then the suspension was gently vortexed. For the negative control, sterile PBS without bacteria was used. The mixtures were incubated at room temperature in 1.5 mL plastic centrifuge tubes and shaken for 40 min. After magnetic separating and washing, 10 μL of TMB (10 mg·mL^{-1}) was added to each tube. The absorption spectrum of the solution was measured with a UV-Vis spectrophotometer in the range 500–750 nm interval.

Detection of real samples

To test the usefulness of our approach for detection in food samples, oyster was purchased from a local supermarket. The food samples contaminated with *V. parahaemolyticus* were prepared as follow: a total of 5 g of oyster was ground and mixed with 5 mL of sterilized PBS to form oyster homogenate. The mixture was filtered through 0.22 μm filter, and the filtrate was collected and inoculated with *V. parahaemolyticus* at concentrations of 10, 50, 100, 300, 500 cfu·mL^{-1}. In contrast, the negative control of blank sample was also prepared in a similar way and tested to investigate the matrix effect of the oyster content in the absorbance measuring system. The detection protocol was as described in section detection of *V. parahaemolyticus*, except that oyster samples were replaced by pure PBS.

Results and discussion

Principle of the colorimetric assay for *V. parahaemolyticus*

The whole procedure of our bare eye assay is limned in Fig. 1. In the present study, MNP-CA was modified with IgG antibodies to act as the capture probe. BSA-MnO_2 NPs were coated with IgY antibodies to act as signal amplifiers. In the presence of *V. parahaemolyticus*, MNP-CA-IgG and IgY-BSA-MnO_2 NPs can recognize and bound to the target at different specific binding sites, leading to the sandwich-type immunocomplexes formed. With an extra magnetic field, unbound IgY-BSA-MnO_2 NPs were removed. In the addition of TMB, the MnO_2 nanoparticles on the sandwich complexes would trigger the oxidation of TMB. The catalytic activity would drastically enhanced in proportion to the *V. parahaemolyticus* concentration. The oxidation reaction was pronounced producing different shades of colors ranging from light to deep blue that were available for bare eye discerning.

Characterization of the MNP-CA-IgG and IgY-BSA-MnO_2 NPs

The size distribution and morphology characteristics of MNP-CA and MNP-CA-IgG are shown in Fig. 2a, b. The MNP-CA and MNP-CA-IgG were well dispersed roughly spherical nanoparticles. Compared to MNP-CA, the average size of MNP-CA-IgG slightly increased from 218.2 nm to about 242.7 nm estimated with a Nano Measurer (version 1.2) [24], indicating the IgG antibodies were coated onto the MNP-CA surface. The FTIR spectrum of MNP-CA (black curve) and (red curve) is shown in Fig. 2c and exhibits various characteristic bands of O-H, C = O, and C-H vibrations. Besides, several new characteristic peaks of protein were observed from the spectrum of MNP-CA-IgG. Especially, the band at around 1650 cm^{-1} (amide I) was assigned to the C = O stretching vibration of peptide linkages [25], demonstrating that the antibodies are conjugated on the MNP-CA surface. Moreover, magnetic measurement revealed that the saturation magnetization of MNP-CA and MNP-CA-IgG is 54.3 emu·g^{-1} and 54.4 emu·g^{-1}, respectively, while the coercivity and remanence magnetization are almost zero (Fig. S2). All these results implied that MNP-CA-IgG were expectedly obtained with excellent superparamagnetic properties, which enabled them to have a quick magnetic response. Besides, TEM imaging (Fig. 2d) was performed to demonstrate the conjugation of MNP-CA-IgG with *V. parahaemolyticus*. It shows several MNP-CA-IgG (black spots) bound to one *V. parahaemolyticus*, facilitating the effective capture by a simple magnetic scaffold.

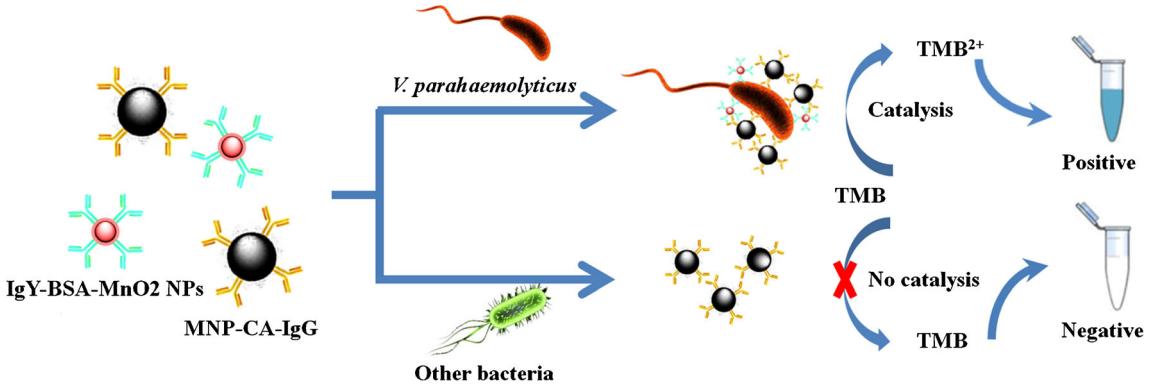

Fig. 1 Schematic diagram for immunomagnetic capture and colorimetric detection of *V. parahaemolyticus*

For characterization of IgY-BSA-MnO_2 NPs, The TEM, zeta potential and FTIR techniques were used. TEM images (Fig. S3a and Fig. S3b) display BSA-MnO_2 NPs and IgY-BSA-MnO_2 NPs were predominantly spherical in shape and highly dispersed, which was similar with the result obtained in previous study [15]. After conjugated with IgY antibodies, the zeta potential values of IgY-BSA-MnO2 NPs displayed a significant increase from −24.01 to −16.41 mv at pH = 7.0 (Fig. S3c). This phenomenon demonstrated that the negative charge of BSA-MnO_2 NPs can be neutralized by the conjugation of IgY antibodies, because the isoelectric point of IgY is around 6.7 greater than that of BSA (pI = 4.7) [26]. In addition, Fig. S3d shows the FTIR spectrum of BSA-MnO_2 NPs (black curve) and IgY-BSA-MnO_2 NPs (red curve). Attributing to the introduction of IgY to BSA-MnO_2 NPs, the O-H, N-H (3400 cm^{-1}), and C = O (1650 cm^{-1}) stretching vibrational bands were enhancement. These results demonstrated that IgY antibodies were successfully coated on BSA-MnO_2 NPs. Furthermore, IgY-BSA-MnO_2 NPs can oxidize TMB to produce a deep blue colour within 5 min (Fig. S3e). This result provided direct evidence that IgY-BSA-MnO_2 NPs exhibited a remarkable oxidase-like activity to generate strong colorimetric signals quickly.

Optimization of experimental conditions

According to the principle of the assay, the MNP-CA-IgG concentration was firstly optimized by using 10^5 cfu·mL^{-1} of *V. parahaemolyticus* as a model. Compared to the typical photograph of the colonies formed by *V. parahaemolyticus* in the Fig. S4 g, it can be seen that the number of colony-forming units was gradually decreased with the increased concentration of the MNP-CA-IgG (Fig. S4a-S4f). Based on the plate

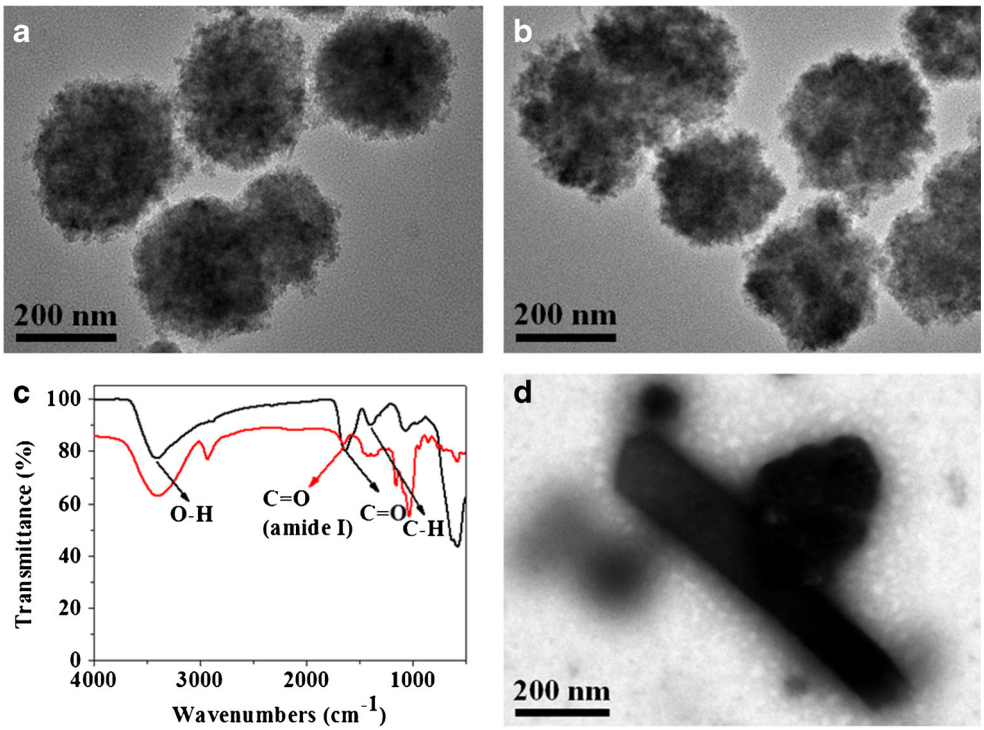

Fig. 2 Characterization of MNP-CA and MNP-CA-IgG: **a** TEM image of MNP-CA prepared by a solvothermal method. **b** MNP-CA after functionalized with IgG antibodies. **c** UV-Vis spectra of MNP-CA (black line) and MNP-CA-IgG (red line). **d** TEM image of *V. parahaemolyticus* captured by MNP-CA-IgG

count method [23], the capture efficiencies of *V. parahaemolyticus* were calculated. As shown in Table S1, the maximum of capture efficiency was attained at 0.5 mg·mL^{-1} MNP-CA-IgG, where 91.3% of the bacteria were captured. Further increase in MNP-CA-IgG concentration, it had very little additional beneficial effect. Therefore, 0.5 mg·mL^{-1} of MNP-CA-IgG was chosen for all of the following experiments. To measure the saturation concentration of IgY-BSA-MnO_2 NPs binding to bacteria, the absorption of oxidized TMB was recorded by a direct ELISA method. As shown in Fig. S5, the absorption of oxidized TMB increased dramatically with the increasing concentration of the IgY-BSA-MnO_2 NPs until it reached 1.0 mg·mL^{-1}, and thereafter, almost no increased was observed. Therefore, 1.0 mg·mL^{-1} IgY-BSA-MnO_2 NPs were used for the following experiments. Eventually, the incubation time was also optimized by record the absorption of oxidized TMB with different test intervals. The oxidized TMB absorption gradually increased during the first 40 min incubation, where thereafter, even slightly decreased was observed (Fig. S6). In summary, the detection system composed of 0.5 mg·mL^{-1} MNP-CA-IgG and 1.0 mg·mL^{-1} IgY-BSA-MnO_2 NPs with incubation time of 40 min were chosen in the present work to achieve the best colorimetric performance.

Sensitive detection of *V. parahaemolyticus*

As mentioned above, the color signal was produced via the enzymatic oxidation of TMB by using IgY-BSA-MnO_2 NPs as an "artificial oxidase". The saturated IgY-BSA-MnO_2 NPs were anchored on the surface antigen of *V. parahaemolyticus*, so the color signal should be dependent upon the concentration of target bacteria. To demonstrate performance of the detection strategy, various concentrations of *V. parahaemolyticus* ranging from 10 to 10^5 cfu·mL^{-1} were experimented using optimal assay conditions. As shown in Fig. 3a, with increasing of the concentration of *V. parahaemolyticus* after 10 min coloration time, the solution colour gradually changed from light to deep blue. Similar changes in UV-Vis spectra were recorded at 652 nm, the absorbance value was enhanced with *V. parahaemolyticus* concentration increased from 10 to 10^5 cfu·mL^{-1} (Fig. 3b). In addition, the intensities of absorbance at 652 nm were found to increase linearly with the concentration of *V. parahaemolyticus* from 10 to 10^5 cfu·mL^{-1}, and the regression equation for the calibration curve was $A_{652\ nm}$ = 0.168lgC + 0.244, with R^2 = 0.997 (Fig. 3c), where C is the *V. parahaemolyticus* count in cfu·mL^{-1}. Even though the samples with just 10 cfu·mL^{-1} of *V. parahaemolyticus* present show distinct differences from the control sample containing no bacteria, indicating that the limit of detection (LOD) for this analytical procedure was calculated to be 10 cfu·mL^{-1}, at which the value of absorbance is three-fold higher than those of control group. The Chinese National standards for allowable levels of *V. parahaemolyticus* in aquatic products and aquatic seasoning are less than 100 cfu·mL^{-1} [27], and the LOD and linear range in our protocol meets these requirements.

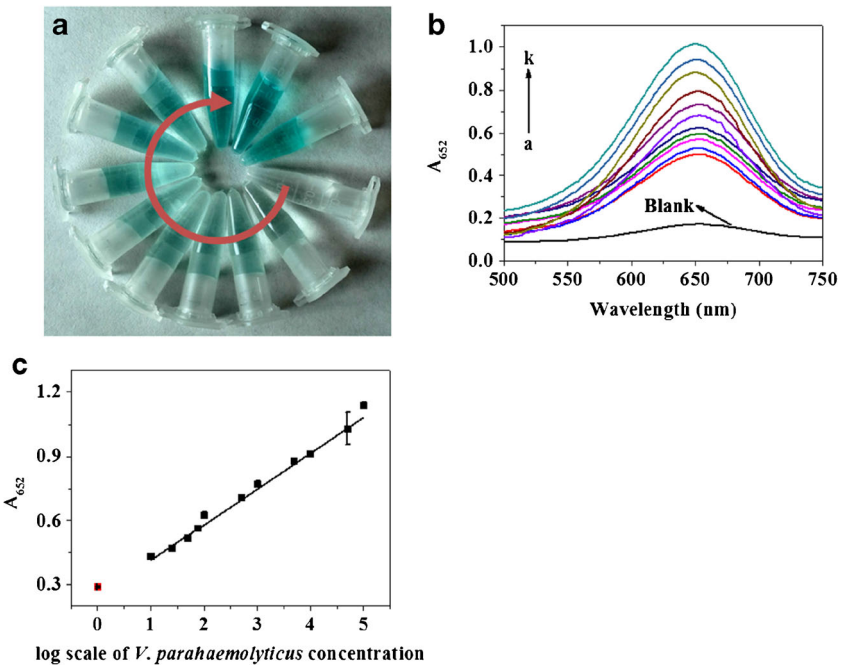

Fig. 3 (**a**) Visual and (**b**) UV-Visible spectra of detection system after incubation with *V. parahaemolyticus* at various concentrations (a → k: 0, 10, 25, 50, 75, 100, 500, 1000, 5000, 10,000, 50,000 and 100,000 cfu·mL^{-1}). (**c**) The calibration curve for *V. parahaemolyticus* ($A_{652\ nm}$ vs. the logarithm of *V. parahaemolyticus* concentration). The maximum absorption wavelength is 652 nm. Error bars represent the standard deviation of three replicates

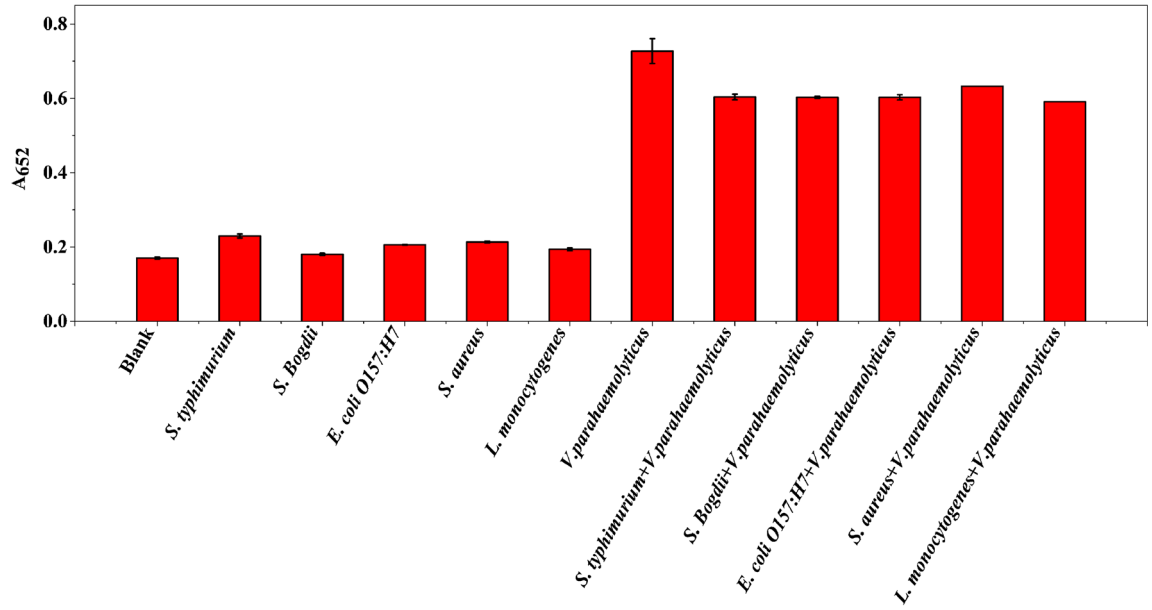

Fig. 4 Selectivity test. Absorbance signal of detection system in the absence of any strains (blank) and after incubation with different bacteria (*V. parahemolyticu* at 100 cfu·mL^{-1}, each species of other bacteria at 1000 cfu·mL^{-1}). (The maximum absorption wavelength is 652 nm) Error bars represent the standard deviation of three replicates

Specificity of the colorimetric assay

To investigate the selectivity of our colorimetric method for *V. parahaemolyticus*, other common bacteria strains, such as *S. typhimurium*, *S. bogdii*, *E. coli O157:H7*, *S. aureus* and *L. monocytogenes* (each at 1000 cfu·mL^{-1}), were employed as negative samples, and the PBS sample was set as reagent blank. The various kinds of negative samples can generate different signal intensities under the same conditions. However, there was no statistical significant difference in absorbance values between the negative samples and reagent control (Fig. 4). For the target bacteria, a significant change in absorbance signal was observed when the detection system was incubated with 100 cfu·mL^{-1} of *V. parahaemolyticus*. Therefore, we can conclude that the good specificity was attributed to the highly selective and specific binding between *V. parahaemolyticus* and its specific antibodies. Especially, when *V. parahaemolyticus* was mixed with other bacteria up to the ratio of 1:10, the absorbance intensity of the detection system displayed a noticeable increase, similar to those of *V. parahaemolyticus* alone (Fig. 4). These results proved that the method was highly specific for *V. parahaemolyticus* and can distinguish *V. parahaemolyticus* from other bacteria.

Analysis of real samples

To further investigate the accuracy of the method, the recovery of *V. parahaemolyticus* in real food samples were analyzed. The standard calibration curve for oyster samples was established by mixing the different concentrations of *V. parahaemolyticus* in the spiked samples (Fig. S7). Probably due to the protein contents verified in food matrices, the parameters of the calibration curve differed from those of PBS sample including both slope and intercept terms. Despite of this, the sensitivity of oyster samples was not interfered, which imply that the setup method can be applied in complex matrix. Simultaneously, the 100 cfu·mL^{-1} of *V. parahaemolyticus* spiked into samples was determined with three replicates and the recovery tests were summarized in Table 1. The recoveries were in the range of 87.5–106.0%. These results indicated that the accuracy and precision of our analytical method were applicable for colorimetric detection without pre-enrichment and complicated operation. Compared to many different detection methods for *V. parahaemolyticus*, such as electrochemical biosensor [28] and surface-enhanced raman scattering (SERS) biosensor [29] (see Supplementary Material, Table S2), our method has superior properties for visual detection of *V. parahaemolyticus*.

Table 1 The recovery and RSD value of detecting *V. parahemolyticus* in spiked food samples ($\bar{x}\pm s$, $n = 3$)

Samples	Found (cfu·mL^{-1})	Added (cfu·mL^{-1})	Recovered (cfu·mL^{-1})	Recovery (%)	RSD (%)
1	BDL[a]	100	106.0 ± 5.7	106.0	5.4
2	BDL	100	96.5 ± 4.9	96.5	5.1
3	BDL	100	87.5 ± 3.5	87.5	4.0

[a] *BDL* below detection limit

Conclusion

In summary, a robust colorimetric assay was developed for highly sensitive and selective detection of *V. parahaemolyticus* in foods using magnetic beads-based sandwich immunoassay coupling with artificial enzyme-mediated signal amplification. Taking advantages of the superior capture efficiency and catalytic activity, *V. parahaemolyticus* can be readily detected with a low detection limit (10 cfu·mL^{-1}) and a wide line arrange from 10 to 10^5 cfu·mL^{-1} under the optimum conditions. In additional, this visual detection assay was verified to be compatible with food samples, benefited from high specificity and selectivity. Therefore, we envision that the colorimetric assay will be widely applicable for rapid detection of a wide variety of other bacteria and pathogens.

Acknowledgements All the authors acknowledge the Jilin University shared instrumentation facility, and School of Public Health, Jilin University for providing bacteria. This work was supported by the Chinese National Natural Science Foundation (Grant No. 81473018, 81602894, and 81602895) and China Postdoctoral Science Foundation (2017 T100214, 2016 M591492).

Compliance with ethical standards The author(s) declare that they have no competing interests.

References

1. Huehn S, Eichhorn C, Urmersbach S, Breidenbach J, Bechlars S, Bier N, Alter T, Bartelt E, Frank C, Oberheitmann B, Gunzer F, Brennholt N, Böer S, Appel B, Dieckmann R, Strauch E (2014) Pathogenic vibrios in environmental, seafood and clinical sources in Germany. Int J Med Microbiol 304(7):843–850
2. Su YC, Liu C (2007) *Vibrio parahaemolyticus*: a concern of seafood safety. Food Microbiol 24(6):549–558
3. Broberg CA, Calder TJ, Orth K (2011) *Vibrio parahaemolyticus* cell biology and pathogenicity determinants. Microbes Infect 13(12-13):992–1001
4. DePaola A, Kaysner CA, Bowers J, Cook DW (2000) Environmental Investigations of *Vibrio parahaemolyticus* in Oysters after Outbreaks in Washington, Texas, and New York (1997 and 1998). Appl Environ Microbiol 66(11):4649–4654
5. Drake SL, DePaola A, Jaykus LA (2007) An Overview of *Vibrio vulnificus* and *Vibrio parahaemolyticus*. Compr Rev Food Sci F 6(4):120–144
6. Di H, Ye L, Neogi SB, Meng H, Yan H, Yamasaki S, Shi L (2015) Development and evaluation of a loop-mediated isothermal amplification assay combined with enrichment culture for rapid detection of very low numbers of *Vibrio parahaemolyticus* in seafood samples. Biol Pharm Bull 38(1):82–87
7. Park B, Choi SJ (2017) Sensitive immunoassay-based detection of Vibrio parahaemolyticus using capture and labeling particles in a stationary liquid phase lab-on-a-chip. Biosens Bioelectron 90:269–275
8. Zhang Z, Xiao L, Lou Y, Jin M, Liao C, Malakar PK, Pan Y, Zhao Y (2015) Development of a multiplex real-time PCR method for simultaneous detection of *Vibrio parahaemolyticus*, *Listeria monocytogenes* and *Salmonella* spp. in raw shrimp. Food Control 51:31–36
9. Niemz A, Ferguson TM, Boyle DS (2011) Point-of-care nucleic acid testing for infectious diseases. Trends Biotechnol 29(5):240–250
10. Cho IH, Mauer L, Irudayaraj J (2014) In-situ fluorescent immunomagnetic multiplex detection of foodborne pathogens in very low numbers. Biosens Bioelectron 57:143–148
11. Shukla S, Lee G, Song X, Park S, Kim M (2016) Immunoliposome-based immunomagnetic concentration and separation assay for rapid detection of Cronobacter sakazakii. Biosens Bioelectron 77:986–994
12. Chattopadhyay S, Kaur A, Jain S, Sabharwal PK, Singh H (2016) Functionalized polymeric magnetic nanoconstructs for selective capturing and sensitive detection of *Salmonella typhimurium*. Anal Chim Acta 937:127–135
13. Wu S, Wang Y, Duan N, Ma H, Wang Z (2015) Colorimetric aptasensor based on enzyme for the detection of *Vibrio parahemolyticus*. J Agric Food Chem 63(35):7849–7854
14. Liu J, Meng L, Fei Z, Dyson PJ, Jing X, Liu X (2017) MnO_2 nanosheets as an artificial enzyme to mimic oxidase for rapid and sensitive detection of glutathione. Biosens Bioelectron 57:69–74
15. Liu X, Wang Q, Zhao H, Zhang L, Su Y, Lv Y (2012) BSA-templated MnO_2 nanoparticles as both peroxidase and oxidase mimics. Analyst 137(19):4552–4558
16. Yuan J, Cen Y, Kong XJ, Wu S, Liu CL, Yu RQ, Chu X (2015) MnO_2-Nanosheet-Modified Upconversion Nanosystem for Sensitive Turn-On Fluorescence Detection of H_2O_2 and Glucose in Blood. ACS Appl Mater Interfaces 7(19):10548–10555
17. Yu H, Zheng L (2016) Manganese dioxide nanosheets as an optical probe for photometric determination of free chlorine. Microchim Acta 183(7):2229–2234
18. Liu Y, Zhao C, Fu K, Song X, Xu K, Wang J, Li J (2017) Selective turn-on fluorescence detection of *Vibrio parahaemolyticus* in food based on charge-transfer between CdSe/ZnS quantum dots and gold nanoparticles. Food Control 80:380–387
19. Song D, Qu X, Liu Y, Li L, Yin D, Li J, Xu K, Xie R, Zhai Y, Zhang H, Bao H, Zhao C, Wang J, Song X, Song W (2017) A Rapid Detection Method of *Brucella* with Quantum Dots and Magnetic Beads Conjugated with Different Polyclonal Antibodies. Nanoscale Res Lett 12(1):179
20. Fan K, Wang H, Xi J, Liu Q, Meng X, Duan D, Gao L, Yan X (2016) Optimization of Fe_3O_4 nanozyme activity via single amino acid modification mimicking an enzyme active site. Chem Commun 53(2):424–427
21. Li F, Zhao Q, Wang C, Lu X, Li XF, Le XC (2010) Detection of *Escherichia coli O157:H7* using gold nanoparticle labeling and inductively coupled plasma mass spectrometry. Anal Chem 82(8):3399–3403
22. Wen CY, Jiang YZ, Li XY, Tang M, Wu LL, Hu J, Pang DW, Zeng JB (2017) Efficient Enrichment and Analyses of Bacteria at Ultralow Concentration with Quick-Response Magnetic Nanospheres. ACS Appl Mater Interfaces 9(11):9416–9425
23. Retnakumari A, Setua S, Menon D, Ravindran P, Muhammed H, Pradeep T, Nair S, Koyakutty M (2010) Molecular-receptor-specific, non-toxic, near-infrared-emitting Au cluster-protein nanoconjugates for targeted cancer imaging. Nanotechnology 21(5):055103
24. Wang W, Wang Z, Liu J, Luo Z, Suib SL, He P, Ding G, Zhang Z, Sun L (2017) Single-step One-pot Synthesis of TiO2 Nanosheets Doped with Sulfur on Reduced Graphene Oxide with Enhanced Photocatalytic Activity. Sci Rep 7:46610

25. Gao Z, Xu M, Hou L, Chen G, Tang D (2013) Irregular-shaped platinum nanoparticles as peroxidase mimics for highly efficient colorimetric immunoassay. Anal Chim Acta 776:79–86
26. Dávalos-Pantoja L, Ortega-Vinuesa JL, Bastos-González D, Hidalgo-Alvarez R (2000) A comparative study between the adsorption of IgY and IgG on latex particles. J Biomater Sci Polym Ed 11(6):657–673
27. Duan N, Yan Y, Wu S, Wang Z (2016) *Vibrio parahaemolyticus* detection aptasensor using surface-enhanced Raman scattering. Food Control 63:122–127
28. Teng J, Ye Y, Yao L, Yan C, Cheng K, Xue F, Pan D, Li B, Chen W (2017) Rolling circle amplification based amperometric aptamer/immuno hybrid biosensor for ultrasensitive detection of *Vibrio parahaemolyticus*. Microchim Acta 184(9):3477–3485
29. Duan N, Shen M, Wu S, Zhao C, Ma X, Wang Z (2017) Graphene oxide wrapped Fe3O4@Au nanostructures as substrates for aptamer-based detection of *Vibrio parahaemolyticus* by surface-enhanced Raman spectroscopy. Microchim Acta 184(8):2653–2660